Photocarrier Transfer Across Monolayer MoS_2-$MoSe_2$ Lateral Heterojunctions

Matthew Z. Bellus,[†] Masoud Mahjouri-Samani,[‡,¶] Samuel D. Lane,[†] Akinola D. Oyedele,[‡,§] Xufan Li,[‡] Alexander A. Puretzky,[‡] David Geohegan,[‡] Kai Xiao,[‡] and Hui Zhao[*,†]

†*Department of Physics and Astronomy, The University of Kansas, Lawrence, Kansas 66045, United States*

‡*Center for Nanophase Materials Sciences, Oak Ridge National Laboratory, Oak Ridge, Tennessee 37831, United States*

¶*Electrical and Computer Engineering, Auburn University, Auburn, AL 36849, United States*

§*Bredesen Center for Interdisciplinary Research and Graduate Education, University of Tennessee, Knoxville, Tennessee 37996, United States*

E-mail: huizhao@ku.edu

Abstract

In-plane heterojuctions formed from two monolayer semiconductors represent the finest control of electrons in condensed matter, and has attracted significant interests. Various device studies have shown the effectiveness of such structures to control electronic processes, illustrating their potentials for electronic and optoelectronic applications. However, information about the physical mechanisms of charge carrier transfer across the junctions is still rare, mainly due to the lack

of adequate experimental techniques. Here we show that transient absorption measurements with high spatial and temporal resolution can be used to directly monitor such transfer processes. We studied MoS_2-$MoSe_2$ in-plane heterostructures fabricated by chemical vapor deposition and lithographic patterning followed by laser generated vapor sulfurization. Transient absorption measurements in reflection geometry revealed evidence of exciton transfer from MoS_2 to $MoSe_2$. By comparing the experimental data with a simulation, we extracted an exciton transfer velocity of 10^4 m s^{-1}. These results provide valuable information for understanding and controlling in-plane carrier transfer in two-dimensional lateral heterostructures for their electronic and optoelectronic applications.

KEYWORDS: van der Waals interface, transition metal dichalcogenide, electron transfer, transient absorption, two-dimensional material

Recently, two-dimensional (2D) materials have drawn considerable attention.[1–3] For example, several interesting properties have been discovered in semiconducting transition metal dichalcogenides (TMDs), such as layer-sensitive electronic structures,[4,5] valley-selective optical coupling,[6–8] extremely large exciton binding energies,[9,10] and strong nonlinear optical responses.[11–13] In addition to their potential applications as monolayer semiconductors,[14–17] their ultimate thinness offers high degrees of control of electrons at atomic length scales. Vertically stacked van der Waals heterostructures have been extensively studied, where efficient interlayer electron transfer and the control of layer population of electrons and holes have been demonstrated.[18–22] Unlike in heterostructures formed by ionic or covalent materials, the lattice matching requirement is relaxed in these van der Waals materials. As a result, a large number of combinations of 2D materials can be explored to form multilayer materials with tailored properties for targeted applications.

An equally - if not more - intriguing opportunity offered by 2D materials is to control electrons in-plane by utilizing *lateral* heterostructures formed by two 2D materials. Lat-

eral modulation of electronic and optical properties of 2D materials is necessary for planar devices with high-density integration potentials, such as atomically thin p-n junctions, light-emitting diodes, and photovoltaic devices. Since 2014, several groups have reported bottom-up fabrication of lateral heterostructures, such as chalcogen-changing MoS_2-$MoSe_2$[23] and WS_2-WSe_2,[23,24] and metal-changing MoS_2-WS_2[24–28] and $MoSe_2$-WSe_2.[29] These TMD lateral heterostructures have high-quality interfaces and coherent lattices of the two materials. Furthermore, using two-step epitaxy growth, it is possible to fabricate heterostructures with both chalcogen and metal atoms changing, such as WSe_2-MoS_2, where alloy formation in the junction region can be avoided, and the shape of the junction can be precisely controlled.[30] Patterned growth of lateral heterostructures utilizing lithography[31] or focused ion beam etching[32,33] has also been demonstrated, illustrating the potential of device integration.

The successful fabrication of lateral heterostructures enabled studies of electron transfer across the junctions, a core issue for their applications in electronics and optoelectronics. It was found that, in general, TMD lateral heterostructures form type-II band alignments, which facilitate separation of electrons and holes.[34–36] When the two materials forming a heterostructure have different types of charge carriers, effective p-n junctions can form, as confirmed by observations of current rectification and photovoltaic effects.[23,25,27,30,37]

Although these pioneer studies have revealed the effectiveness of electron transport in these materials, quantitative information on mechanisms of this process is rare. Here we report a temporally and spatially resolved study of photocarrier transport across lateral junctions formed by MoS_2 and $MoSe_2$ monolayers (MLs). We found that photocarriers injected in the MoS_2 side of the junction transfer to the $MoSe_2$ side with a velocity of about 10^4 m s^{-1} at room temperature. The transfer occurs for several tens of picoseconds over a distance on the order of 100 nm. We also obtain evidence that both electrons and holes transfer to $MoSe_2$, which is consistent with the predicted type-I band alignment.

Results/Discussion

The MoS_2-$MoSe_2$ lateral heterostructure was schematically illustrated in Figure 1(a). The samples were formed by the local conversion of $MoSe_2$ to MoS_2 within a ML crystal synthesized by chemical vapor deposition, as reported in Ref. 31. First, $MoSe_2$ MLs were grown. Then, different sized SiO_2 strips were patterned on $MoSe_2$ MLs by using e-beam lithography and e-beam evaporation.[31] A sulfurization process based on laser vaporization of a sulfur target was then used to convert exposed areas, not covered by SiO_2, from $MoSe_2$ to MoS_2.[31] Figure 1(b) shows an optical microscope image of a lateral heterostructure sample, which has alternating MoS_2 and $MoSe_2$ strips of 7-μm wide. The blueish color strips are $MoSe_2$ areas covered with about 50-nm thick SiO_2. The uncovered areas are converted MoS_2 after the sulfurization process. The wide strips provide isolated areas of each material for a direct comparison of properties, as well as the ability to probe the behavior of a single junction. We note that because $MoSe_2$ is covered by SiO_2, its properties could be different from uncovered $MoSe_2$ due to the dielectric screening effect of SiO_2.

To study the photocarrier dynamics, we utilized transient absorption measurements in reflection geometry.[38] Pump and probe laser pulses, of about 100 fs in duration, were focused onto the sample through an objective lens. We measure the differential reflection, which is defined as $\Delta R/R_0 = (R - R_0)/R_0$, with R and R_0 representing the reflectance of the probe from the sample with and without the presence of the pump, respectively (see Methods). When $\Delta R/R_0 \ll 1$, this quantity is proportional to the change of the absorption coefficient by the pump-injected photocarriers.[39] In the measurements, the probe is tuned to the A-exciton resonance of the sample. Generally speaking, photocarriers can exist in forms of free electron-hole pairs or excitons. Both types of photocarriers can induce changes of the excitonic absorption peak by mechanisms such as phase-space state filling,[40] screening of the Coulomb interaction,[40] and bandgap renormalization.[41] Hence, the differential reflection signal can be induced by either free electron-hole pairs or excitons, or both. Since excitons in 2D TMDs have large binding energies[9,10,42] and are stable at room temperature, we attribute

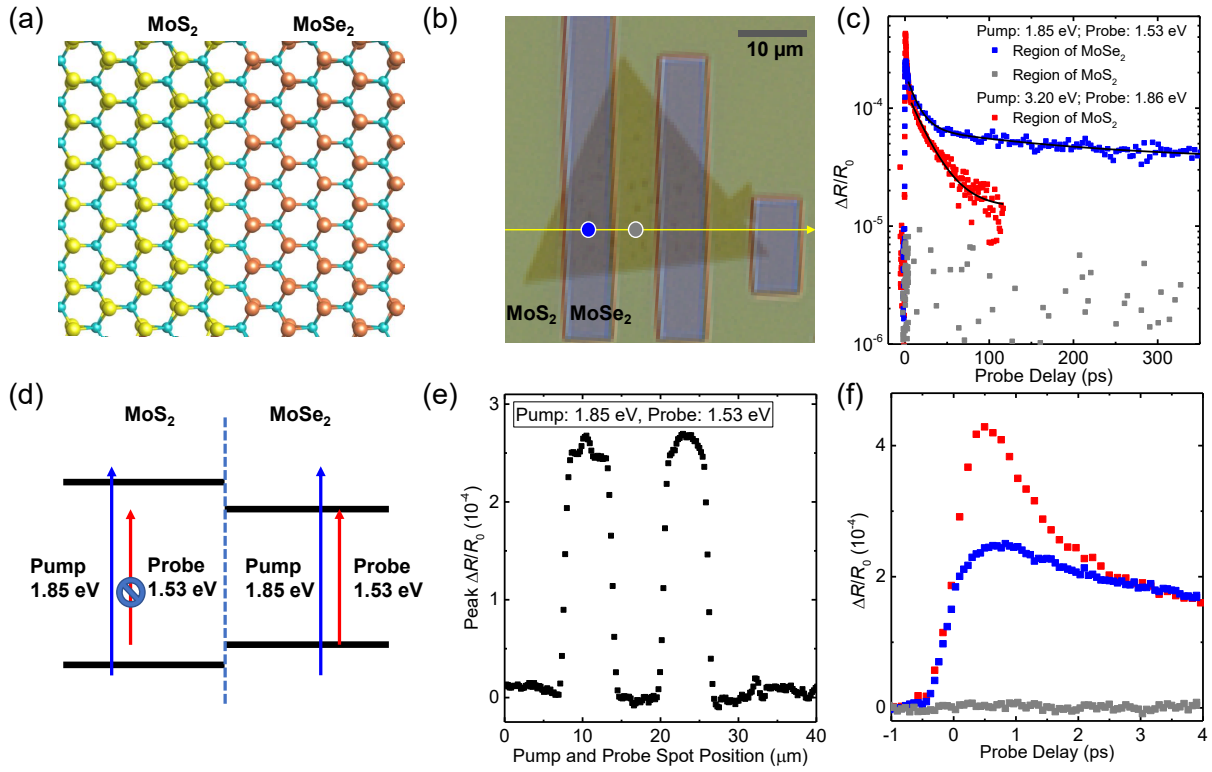

Figure 1: (a) Schematic illustration of the MoS_2-$MoSe_2$ lateral heterojunction (b) Optical image of the MoS_2-$MoSe_2$ lateral heterostructure sample with 7-μm strips of each material. (c) Differential reflection signal obtained from different locations of the sample and with different pump-probe configurations as indicated in the legend. (d) Band alignment and pump-probe schemes. (e) Peak differential reflection signal, of a 1.53 eV probe, as a function of sample position. (f) Same as (c) but showing early probe delays.

the signal to the excitons after they are formed. Under the low-density regimes, the signal is approximately proportional to the exciton density.[38]

We started by locating the pump and probe laser spots in a region of $MoSe_2$, as shown by the blue circle in Figure 1(b). As shown schematically in Figure 1(d), the probe pulse with a photon energy of 1.53 eV is tuned to the A-exciton resonance of $MoSe_2$.[31] The 1.85-eV pump with an energy fluence of about 20 μJ cm^{-2} excites a peak carrier density of about 10^{12} cm^{-2}, which is estimated by using an absorption coefficient of 2×10^5 cm^{-1}.[43] The measured differential reflection signal is shown by the blue symbols in Figure 1(c) and (f) for long and short time ranges, respectively. The signal rise to a peak within a time limited

by the instrument response time. This indicates that the injected carriers induce a transient absorption signal at the exciton resonance instantaneously, a feature generally observed in 2D TMDs.[38] The decay of the signal was fit by a biexponential function, $\Delta R/R_0 = A_1\exp(-t/\tau_1) + A_2\exp(-t/\tau_2) + A_0$, as shown by the fit curve. The two decay constants are $\tau_1 = 13 \pm 1$ and $\tau_2 = 190 \pm 50$ ps, respectively, with $A_1 : A_2 \approx 4 : 1$. We attribute the long time constant to the exciton lifetime. The short time constant could originate from effects of exciton-exciton annihilation,[44,45] hot excitons, or other mechanisms.[46,47] We repeated the measurement with the laser spots on the MoS_2 region [gray circle in Figure 1(b)]. No signal was detected, as indicated by the gray symbols in Figure 1(c). With an absorption coefficient of 3.5×10^5 cm^{-1}, the pump is expected to inject carriers in MoS_2 with a density of 1.8×10^{12} cm^{-2}. The lack of the signal is expected, since the probe photon energy is below the exciton resonance of MoS_2. To further confirm that the probe is insensitive to carriers in MoS_2, we measure the peak differential reflection signal as we scan the laser spots along the yellow line in Figure 1(b). The results [Figure 1(e)] clearly show that only $MoSe_2$ regions produce a signal. It is also important to note that a portion of the deposited SiO_2, only covering the substrate, is measured in this scan, which expectedly produces no signal. This proves that the signal we see from $MoSe_2$ is indeed from $MoSe_2$ and not from the protective SiO_2 layer.

Considering that MoS_2 samples were fabricated by sulfurization of $MoSe_2$, it is necessary to probe the photocarrier dynamics in MoS_2. For this purpose, we measured the differential reflection of a 1.86-eV probe, which is located on MoS_2 and tuned to the A-exciton resonance of MoS_2, with a pump of 3.20 eV. The result is shown by the red symbols in Figure 1(c) and (f). The signal also rise to a peak within a time limited by the instrument response time. An initial fast decay of the signal of about 1 ps was observed, which represents a short transient process as free-carriers form excitons.[48,49] The decay of the signal can be fit by a single exponential function, $\Delta R/R_0 = A\exp(-t/\tau) + A_0$, with a decay constant of 24 ± 2 ps. This exciton lifetime is comparable to exfoliated MoS_2 MLs,[38,50] confirming the high quality

of MoS_2 fabricated by this method.

Next, we focus on the junction between these two materials and the expected photocarrier transfer from MoS_2 to $MoSe_2$. The left column of Figure 2 illustrates the experimental scheme. According to first-principle calculations,[31] the MoS_2-$MoSe_2$ lateral heterostructures forms a type-I band alignment with both the bottom of the conduction band and the top of the valence band located in the $MoSe_2$ layer, as illustrated in Figure 2(a). When the sample is excited by an ultrashort laser pulse (vertical blue arrow), electrons-hole pairs in MoS_2 quickly form excitons on a picosecond time scale.[48,49] Due to their large binding energies of several hundred meV,[42] excitons are stable, and move as a whole. Figure 2(b) shows in real space that the tightly focused laser spot (dashed circle) located at the junction produces excitons on both sides of the junction. The vertical line, in the middle of the laser spot, represents the center of the exciton density profile. Due to the type-I band alignment, the excitons in MoS_2 (yellow circles) are expected to transfer to $MoSe_2$. After the transfer, the density of excitons in the region of $MoSe_2$ near the junction increases, as illustrated in Figure 2(c). This causes the center of the density profile in $MoSe_2$ to shift toward the junction.

To study this transfer process, we measured the differential reflection of the 1.53 eV probe as a function of the probe delay and the relative spatial separation between the pump and probe spots. Here, a 2.21-eV pump was focused through an objective lens with a numerical aperture of 0.7 to a spot size of 0.65 μm full width at half maximum (FWHM) with a peak fluence of about 80 μJ cm^{-2}. The probe spot size is about 0.9 μm. Both spot sizes were measured by using an imaging system that is integrated with the setup and calibrated by imaging a target with a known size. Since we are mostly interested in probing transferred excitons, which are near the junction, the probe spot was positioned near the junction, with its center at about 0.1 μm into the $MoSe_2$ side of the junction. The data was acquired by fixing the sample and the probe spot while moving the pump spot step by step across the junction, by tilting a mirror that reflects the pump beam. At each step, the signal was measured as a function of the probe delay. The results are shown in Figure

2(d). The signal shows a clear trend towards the junction (white line) with increasing probe delay. As presented in Figure 2(c), this shift is indicative of exciton transfer from MoS_2 to $MoSe_2$: before transfer, the excitons in MoS_2 are invisible to the 1.53-eV probe. Once transferred, these excitons become visible, and cause an increase of the local density near the junction, which gives the appearance of the shift. As a further confirmation, we repeated the measurement with a pump photon energy that is smaller than the optical bandgap of MoS_2, so that no excitons are injected in MoS_2. No shift of the center of the profiles was observed (See Supporting Information Available online, Figure S1).

We attempt to quantify this transfer process by tracking the peak of the profile as a function of the probe delay. The symbols in Figure 2(e) show some examples of the profiles. To extract the peak position of the profiles, we fit each profile with an asymmetric double sigmoidal function,

$$y = y_0 + \frac{A}{1+\exp(-\frac{x-x_c+0.5w_1}{w_2})} \cdot \left[1 - \frac{1}{1+\exp(-\frac{x-x_c-0.5w_1}{w_3})}\right], \tag{1}$$

where x_c is the center of the profile, w_1 is the full width at half maximum of the profile, and w_2 and w_3 are the variance or width of the left and right sides, respectively. The choice of this function is solely due to the fact that it fits the profile well, as shown by the curves in Figure 2(e). The obtained peak position is shown by the symbols in Figure 2(f). The large shift of x_c towards the junction with increasing probe delay provides strong evidence of exciton transfer from MoS_2 to $MoSe_2$. Further evidence of the transfer is shown in Figure 2(g), where the width of each side of this double sigmoidal fit is tracked as a function of probe delay. It is clearly seen that the left side, trending further into $MoSe_2$, expands, whereas the right side, trending towards the junction remains constant. With the position of the highest exciton density trending towards the junction, but the profile width only expanding away from the junction, this is a clear indication of exciton build-up near the junction.

Due to the complex nature of this experiment originated from the finite size of the pump

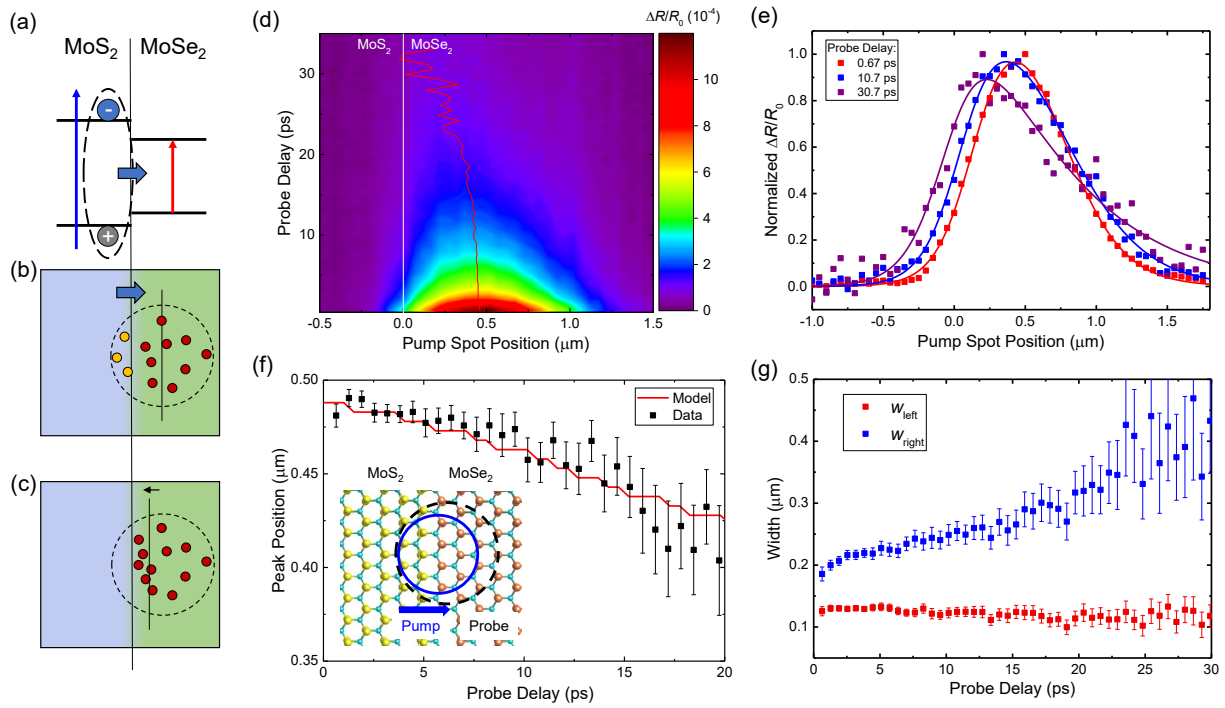

Figure 2: (a) Expected band alignment based on first-principle calculations for the MoS_2-$MoSe_2$ lateral heterostructure. The blue and red vertical arrows represent the pump and probe, respectively. (b) Schematic of the excitons produced in the pump laser spot (dashed circle) in MoS_2 (yellow circles) and $MoSe_2$ sides (red circles) near the junction. The arrow represents the expected direction of exciton transfer based on the band alignment in (a). The vertical line represents the center of the probed exciton density. (c) The exciton density after the expected transfer. The excitons excited in MoS_2 are now in $MoSe_2$, and can be sensed by the probe. The increased density near junction causes a shift of the center of the profile (vertical line) towards the junction. (d) Spatiotemporally resolved differential reflection signal near a single MoS_2-$MoSe_2$ junction. The red line shows the peak signal in time. The 0 position (white line) is defined when the center of the pump spot is at the junction. (e) Examples of normalized spatial profiles with asymmetric double sigmoidal fits. (f) The position of the peak center of each fit as a function of probe delay. The error bars indicate standard deviation of the fits. The red curve is a model with a velocity of about 10^4 m s^{-1}. The inset illustrates the experimental geometry, where the pump spot is located at its 0 position (at the junction) and is scanned across the probe spot with the sample fixed. (g) The width of the left (red) and right (blue) contributions to the fits to the spatial profiles. The error bars indicate standard deviation of the fits.

and probe spots, we next used a model to simulate the observed effect, and to compare it with the experimental data. In this model, we first built the modified Gaussian profiles of the pump and probe based on the measured spot sizes. To account for the fact that the probe is only sensitive to the $MoSe_2$ side of the junction, we constructed a probe sensitivity

function as a Gaussian function (probe intensity profile) multiplied by a Heaviside step function centered at the junction. The initial carrier density profile was constructed by two partial Gaussian profiles (pump spot) that meet at the junction. The amplitudes of each side were set based on the absorption coefficients in each material. Exciton lifetimes and diffusion coefficients measured in the experiment are used to account for the basic dynamics of the carrier density. The model then took the convolution of the pump and probe profiles at each probe delay to mimic the experiment. The details of the model are provided in Supporting Information Available online.

At first, we confirm that without including exciton transfer, the model does not result in any movement of the peak position towards MoS_2 (See Supporting Information Available online, Figure S3). Next, we added an exciton transfer component into the model by allowing the MoS_2 side of the density profile to move linearly in time into $MoSe_2$. This contribution was then added to the $MoSe_2$ side of the density profile. By adjusting the velocity, we found that a good agreement between the data and the model can be achieved with a velocity of 10^4 m s^{-1}, as shown by the red curve in Figure 2(f). We note that this is not the velocity at which the peak shifts. The shift of the peak is an indirect result of exciton movement with this velocity. From the simulation, this velocity results in a transfer length (the distance the transferred excitons move) of 0.35 μm from the junction, which is reasonable considering a diffusion length of about 0.4 μm calculated from the diffusion coefficient and exciton lifetime in $MoSe_2$.[51]

In the analysis, we did not consider effects of defects at the junction area on the photo-carrier dynamics. Our previous study[31] have shown that the defect density at the junction is similar to that inside $MoSe_2$, since the isoelectronic substitution of Se by S (which belong to the same group) does not have much impact to the lattice. Due to the nature of the fabrication technique, the junction is not atomically sharp: there is a few-nanometer region of MoS_xSe_{2-x} alloy between the two materials.[31] Since this region is much smaller than the laser spot, its contribution to the signal is minimal.

Our analysis is based on the assumption that both electrons and holes transfer from MoS_2 to $MoSe_2$ in an excitonic transfer process. This is consistent with the theoretical prediction of type-I band alignment of the heterostructure,[31] It is desirable to provide experimental confirmation on the lack of charge separation. However, it is difficult to probe this effect in the single-junction measurement because the transferred excitons are a small fraction of the excitons probed. For this purpose, we studied a sample with much thinner strips of the two materials, so that a larger portion of the injected excitons are near to junctions and can transfer. Figure 3(a) shows the sample with 500-nm alternating strips of MoS_2 and $MoSe_2$. The sample was excited by a 1.85-eV pump with a spot size of about 1.5 μm. The measured differential reflection of a 1.53-eV probe is shown by the orange symbols in Figure 3(b) and (c). For comparison, the results from $MoSe_2$ ML (blue symbols) are re-plotted from Figure 1. The magnitude of the signal from the heterostructure sample is less than that from ML $MoSe_2$, as expected, since nearly half of the measured area (MoS_2) does not contribute to the signal. The decay of the signal is fit by a biexponential function with two time constants of 14 $\pm$ 9 and 67 $\pm$ 20 ps with comparable contributions.

The lack of a slow component suggests that both electrons and holes transfer. It has been demonstrated that in TMD vertical heterostructures with type-II band alignment, the separation of electrons and holes to different layers can give rise to interlayer excitons with significantly extended lifetimes.[18–22] In the lateral heterostructure studied here, the charge separation would be greater than the vertical heterostructures due to the width of the lateral junction. This should give rise to an extremely long carrier lifetime. Hence, our experimental results indicate that electrons and hole do not separate in this heterostructure, which is consistent with the predicted type-I alignment.[31] This verifies the hypothesis shown in Figure 2(c) that the transferred agents are excitons, instead of individual carriers. Indeed, since the excitons in these materials are formed on a picosecond time scale and are stable at room temperature due to their large binding energies,[9,10,42] it is reasonable that the transfer process of more than 20 ps is dominated by excitons.

Without a net charge transfer, the photocarrier transfer observed here can be classified as an energy transfer process. Generally speaking, energy transfer can be achieved by a Förster process,[52] where an exciton in one material recombines nonradiatively, transferring the energy for the excitation of an electron-hole pair in another material. It can also be accomplished by real-space movement of the exciton across the junction in a Dexters process.[53,54] Efficient Förster process requires a small distance on the order of one nanometer.[55] Given the extend of the charge transfer dimensions here, we expect the process to be dominated by the Dexter mechanism.

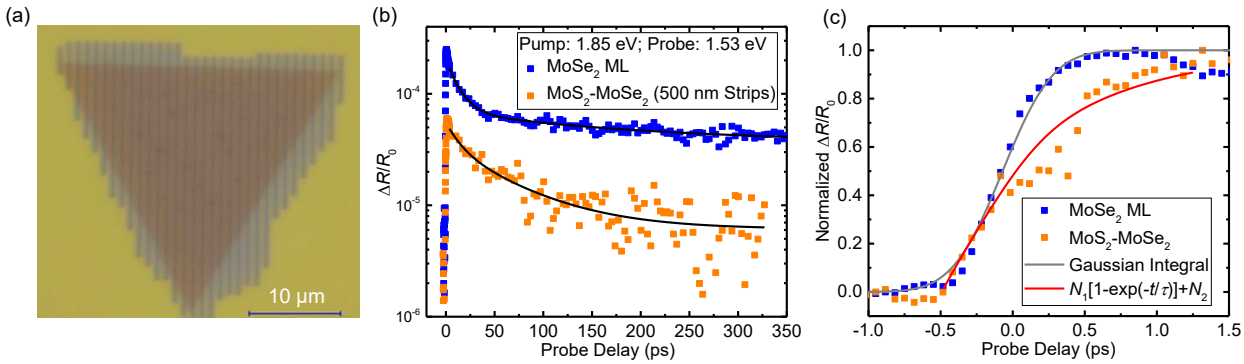

Figure 3: (a) Optical image of the sample with 500-nm alternating strips of MoS_2 and $MoSe_2$. (b) Differential reflection signal of a 1.53-eV probe for the MoS_2-$MoSe_2$ (500-nm strip) sample (orange) and $MoSe_2$ ML (blue). The lines represent biexponential fits to the data. (c) Same as (b), but on a shorter time scale and with the signal normalized. The curves are fits (see text).

Figure 3(c) shows the early part of the dynamics. The signals are normalized for better comparison. Clearly, the rising time of the signal from the heterostructure is slower than from $MoSe_2$ ML. The gray line, fit to the ML $MoSe_2$ data, is calculated using a Gaussian integral with a width of 0.275 ps. This value is close to the width of the cross-correlation of the pump and probe pulses, and thus represents the time resolution of the experimental setup. The red line is a fit by the function $N_1[1 - \exp(-t/\tau_T)] + N_2$, where N_1 and N_2 represent the carrier densities injected in MoS_2 and $MoSe_2$, respectively. Here, τ_T represents the transient time for the signal to reach its peak and is found to be about 0.8 ps. This increased rise time is another evidence of exciton transfer from MoS_2 to $MoSe_2$.

Conclusions

In summary, we have time-resolved exciton transfer across a junction formed by two monolayer semiconductors, MoS_2 and $MoSe_2$. Spatiotemporal measurements of exciton dynamics near a lateral heterojunction revealed evidence of exciton transfer that extended for several tens of picoseconds. A transfer velocity of 10^4 m s^{-1} was deduced by comparing the experimental data with simulations. We also showed that the transferred excitons have a lifetime similar to those in $MoSe_2$ monolayers, suggesting the lack of electron-hole separation, and the type-I nature of the band alignment. These results provide valuable information for understanding and controlling in-plane electron transfer in 2D lateral heterostructures.

Methods

The measurements were performed with a home-made transient absorption microscope. A Ti-sapphire laser (Newport Tsunami) generates 80 MHz and 100-fs pulses with a wavelength tunable from 750 to 850 nm and an average power of 1 W. The output is split to three beams. One beam is used to pump a photonic-crystal fiber to generate a broadband supercontinuum radiation. A band-pass filter is used to select a desired wavelength component from the supercontinuum. Another beam is focused to a beta barium borate crystal for second harmonic generation. The third beam is used directly for the measurements. In each configuration, two of these beams were used as pump and probe. The pump and probe are linearly polarized along perpendicular directions. A beamsplitter is used to combine the two beams and send them to a microscope objective lens. The spot sizes are typically in the range of 0.5 to 2 μm in full-width at half-maximum, depending on the numerical aperture of the objective lens used. The reflected probe is sent to a biased silicon photodiode, the output of which is measured by a lock-in amplifier. A mechanical chopper is used to modulate the pump intensity at about 2 KHz. With this setup, the differential reflection can be measured as a function of the time delay between the pump and probe pulses, which is controlled by

the length of the pump arm, and the location of the pump laser spot, by tilting a mirror in the pump arm.

Acknowledgments

This material is based upon work supported by the National Science Foundation of USA (No. DMR-1505852). The synthesis of materials was supported by the U.S Department of Energy, Office of Science, Basic Energy Sciences, Materials Sciences and Engineering Division. Fabrication and characterization of the samples were conducted at the Center for Nanophase Materials Sciences, which is a DOE Office of Science User Facility.

Supporting Information Available

The following files are available free of charge.

Control experiments performed with no excitation of MoS_2 which shows no shift of the profile peak, discussion on model that simulates the experiments, simulation results showing that peak shift is only observed when an exciton transfer component is included in the model, simulation results that match the experimental data.

References

1. Gibney, E. The Super Materials that Could Trump Graphene. *Nature* **2015**, *522*, 274–276.

2. Neto, A. H. C.; Novoselov, K. New Directions in Science and Technology: Two-Dimensional Crystals. *Rep. Prog. Phys.* **2011**, *74*, 082501.

3. Wang, Q. H.; Kalantar-Zadeh, K.; Kis, A.; Coleman, J. N.; Strano, M. S. Electronics

and Optoelectronics of Two-Dimensional Transition Metal Dichalcogenides. *Nat. Nanotechnol.* **2012**, *7*, 699–712.

4. Mak, K. F.; Lee, C.; Hone, J.; Shan, J.; Heinz, T. F. Atomically Thin MoS_2: A New Direct-Gap Semiconductor. *Phys. Rev. Lett.* **2010**, *105*, 136805.

5. Splendiani, A.; Sun, L.; Zhang, Y.; Li, T.; Kim, J.; Chim, C. Y.; Galli, G.; Wang, F. Emerging Photoluminescence in Monolayer MoS_2. *Nano Lett.* **2010**, *10*, 1271–1275.

6. Xiao, D.; Liu, G. B.; Feng, W.; Xu, X.; Yao, W. Coupled Spin and Valley Physics in Monolayers of MoS_2 and Other Group-VI Dichalcogenides. *Phys. Rev. Lett.* **2012**, *108*, 196802.

7. Zeng, H.; Dai, J.; Yao, W.; Xiao, D.; Cui, X. Valley Polarization in MoS_2 Monolayers by Optical Pumping. *Nat. Nanotechnol.* **2012**, *7*, 490–493.

8. Mak, K. F.; He, K.; Shan, J.; Heinz, T. F. Control of Valley Polarization in Monolayer MoS_2 by Optical Helicity. *Nat. Nanotechnol.* **2012**, *7*, 494–498.

9. Chernikov, A.; Berkelbach, T. C.; Hill, H. M.; Rigosi, A.; Li, Y. L.; Aslan, O. B.; Reichman, D. R.; Hybertsen, M. S.; Heinz, T. F. Exciton Binding Energy and Nonhydrogenic Rydberg Series in Monolayer WS_2. *Phys. Rev. Lett.* **2014**, *113*, 076802.

10. He, K.; Kumar, N.; Zhao, L.; Wang, Z.; Mak, K. F.; Zhao, H.; Shan, J. Tightly Bound Excitons in Monolayer WSe_2. *Phys. Rev. Lett.* **2014**, *113*, 026803.

11. Kumar, N.; Najmaei, S.; Cui, Q.; Ceballos, F.; Ajayan, P. M.; Lou, J.; Zhao, H. Second Harmonic Microscopy of Monolayer MoS_2. *Phys. Rev. B* **2013**, *87*, 161403.

12. Malard, L. M.; Alencar, T. V.; Barboza, A. P. M.; Mak, K. F.; de Paula, A. M. Observation of Intense Second Harmonic Generation from MoS_2 Atomic Crystals. *Phys. Rev. B* **2013**, *87*, 201401.

13. Li, Y.; Rao, Y.; Mak, K. F.; You, Y.; Wang, S.; Dean, C. R.; Heinz, T. F. Probing Symmetry Properties of Few-Layer MoS_2 and h-BN by Optical Second-Harmonic Generation. *Nano Lett.* **2013**, *13*, 3329–3333.

14. Radisavljevic, B.; Radenovic, A.; Brivio, J.; Giacometti, V.; Kis, A. Single-Layer MoS_2 Transistors. *Nat. Nanotechnol.* **2011**, *6*, 147–150.

15. Wang, H.; Yu, L. L.; Lee, Y. H.; Shi, Y. M.; Hsu, A.; Chin, M. L.; Li, L. J.; Dubey, M.; Kong, J.; Palacios, T. Integrated Circuits Based on Bilayer MoS_2 Transistors. *Nano Lett.* **2012**, *12*, 4674–4680.

16. Baugher, B. W. H.; Churchill, H. O. H.; Yang, Y.; Jarillo-Herrero, P. Optoelectronic Devices Based on Electrically Tunable P-N Diodes in a Monolayer Dichalcogenide. *Nat. Nanotechnol.* **2014**, *9*, 262–267.

17. Zhang, Y. J.; Oka, T.; Suzuki, R.; Ye, J. T.; Iwasa, Y. Electrically Switchable Chiral Light-Emitting Transistor. *Science* **2014**, *344*, 725–728.

18. Hong, X.; Kim, J.; Shi, S. F.; Zhang, Y.; Jin, C.; Sun, Y.; Tongay, S.; Wu, J.; Zhang, Y.; Wang, F. Ultrafast Charge Transfer in Atomically Thin MoS_2/WS_2 Heterostructures. *Nat. Nanotechnol.* **2014**, *9*, 682–686.

19. Ceballos, F.; Bellus, M. Z.; Chiu, H. Y.; Zhao, H. Ultrafast Charge Separation and Indirect Exciton Formation in a MoS_2-$MoSe_2$ van der Waals Heterostructure. *ACS Nano* **2014**, *8*, 12717–12724.

20. He, J.; Kumar, N.; Bellus, M. Z.; Chiu, H. Y.; He, D.; Wang, Y.; Zhao, H. Electron Transfer and Coupling in Graphene-Tungsten Disulfide van der Waals Heterostructures. *Nat. Commun.* **2014**, *5*, 5622.

21. Peng, B.; Yu, G.; Liu, X.; Liu, B.; Liang, X.; Bi, L.; Deng, L.; Sum, T. C.; Loh, K. P. Ultrafast Charge Transfer in MoS_2/WSe_2 P-N Heterojunction. *2D Mater.* **2016**, *3*, 025020.

22. Ceballos, F.; Ju, M. G.; Lane, S. D.; Zeng, X. C.; Zhao, H. Highly Efficient and Anomalous Charge Transfer in van der Waals Trilayer Semiconductors. *Nano Lett.* **2017**, *17*, 1623–1628.

23. Duan, X.; Wang, C.; Shaw, J. C.; Cheng, R.; Chen, Y.; Li, H.; Wu, X.; Tang, Y.; Zhang, Q.; Pan, A.; Jiang, J.; Yu, R.; Huang, Y.; Duan, X. Lateral Epitaxial Growth of Two-Dimensional Layered Semiconductor Heterojunctions. *Nat. Nanotechnol.* **2014**, *9*, 1024–1030.

24. Zhang, X. Q.; Lin, C. H.; Tseng, Y. W.; Huang, K. H.; Lee, Y. H. Synthesis of Lateral Heterostructures of Semiconducting Atomic Layers. *Nano Lett.* **2015**, *15*, 410–415.

25. Gong, Y.; Lin, J.; Wang, X.; Shi, G.; Lei, S.; Lin, Z.; Zou, X.; Ye, G.; Vajtai, R.; Yakobson, B. I.; Terrones, H.; Terrones, M.; Tay, B. K.; Lou, J.; Pantelides, S. T.; Liu, Z.; Zhou, W.; Ajayan, P. M. Vertical and In-Plane Heterostructures from WS_2/MoS_2 Monolayers. *Nat. Mater.* **2014**, *13*, 1135–1142.

26. Bogaert, K.; Liu, S.; Chesin, J.; Titow, D.; Gradecak, S.; Garaj, S. Diffusion-Mediated Synthesis of MoS_2/WS_2 Lateral Heterostructures. *Nano Lett.* **2016**, *16*, 5129–5134.

27. Chen, K.; Wan, X.; Xie, W. G.; Wen, J. X.; Kang, Z. W.; Zeng, X. L.; Chen, H. J.; Xu, J. B.; Ldas, B. V. P. Lateral Built-in Potential of Monolayer MoS_2-WS_2 in-Plane Heterostructures by a Shortcut Growth Strategy. *Adv. Mater.* **2015**, *27*, 6431.

28. Heo, H.; Sung, J. H.; Jin, G.; Ahn, J. H.; Kim, K.; Lee, M. J.; Cha, S.; Choi, H.; Jo, M. H. Rotation-Misfit-Free Heteroepitaxial Stacking and Stitching Growth of Hexagonal Transition-Metal Dichalcogenide Monolayers by Nucleation Kinetics Controls. *Adv. Mater.* **2015**, *27*, 3803–3810.

29. Huang, C.; Wu, S.; Sanchez, A. M.; Peters, J. J.; Beanland, R.; Ross, J. S.; Rivera, P.; Yao, W.; Cobden, D. H.; Xu, X. Lateral Heterojunctions Within Monolayer $MoSe_2$-WSe_2 Semiconductors. *Nat. Mater.* **2014**, *13*, 1096–1101.

30. Li, M. Y.; Shi, Y. M.; Cheng, C. C.; Lu, L. S.; Lin, Y. C.; Tang, H. L.; Tsai, M. L.; Chu, C. W.; Wei, K. H.; He, J. H.; Chang, W. H.; Suenaga, K.; Li, L. J. Epitaxial Growth of a Monolayer WSe_2-MoS_2 Lateral P-N Junction with an Atomically Sharp Interface. *Science* **2015**, *349*, 524–528.

31. Mahjouri-Samani, M.; Lin, M. W.; Wang, K.; Lupini, A. R.; Lee, J.; Basile, L.; Boulesbaa, A.; Rouleau, C. M.; Puretzky, A. A.; Ivanov, I. N.; Xiao, K.; Yoon, M; Geohegan; D. B. Patterned Arrays of Lateral Heterojunctions within Monolayer Two-Dimensional Semiconductors. *Nat. Commun.* **2015**, *6*, 7749.

32. Li, H. N.; Li, P.; Huang, J. K.; Li, M. Y.; Yang, C. W.; Shi, Y. M.; Zhang, X. X.; Li, L. J. Laterally Stitched Heterostructures of Transition Metal Dichalcogenide: Chemical Vapor Deposition Growth on Lithographically Patterned Area. *ACS Nano* **2016**, *10*, 10516–10523.

33. Chen, J. Y.; Zhou, W.; Tang, W.; Tian, B. B.; Zhao, X. X.; Xu, H.; Liu, Y. P.; Geng, D. C.; Tan, S. J. R.; Fu, W.; Loh, K. P. Lateral Epitaxy of Atomically Sharp WSe_2/WS_2 Heterojunctions on Silicon Dioxide Substrates. *Chem. Mater.* **2016**, *28*, 7194–7197.

34. Kang, J.; Sahin, H.; Peeters, F. M. Tuning Carrier Confinement in the MoS_2/WS_2 Lateral Heterostructure. *J. Phys. Chem. C* **2015**, *119*, 9580–9586.

35. Guo, Y. Z.; Robertson, J. Band Engineering in Transition Metal Dichalcogenides: Stacked *Versus* Lateral Heterostructures. *Appl. Phys. Lett.* **2016**, *108*, 233104.

36. Lee, J.; Huang, J. S.; Sumpter, B. G.; Yoon, M. Strain-Engineered Optoelectronic Properties of 2D Transition Metal Dichalcogenide Lateral Heterostructures. *2D Mater.* **2017**, *4*, 021016.

37. Chen, K.; Wan, X.; Wen, J. X.; Xie, W. G.; Kang, Z. W.; Zeng, X. L.; Chen, H. J.;

Xu, J. B. Electronic Properties of MoS_2-WS_2 Heterostructures Synthesized with Two-Step Lateral Epitaxial Strategy. *ACS Nano* **2015**, *9*, 9868–9876.

38. Ceballos, F.; Zhao, H. Ultrafast Laser Spectroscopy of Two-Dimensional Materials beyond Graphene. *Adv. Funct. Mater.* **2017**, *27*, 1604509.

39. Wang, R.; Ruzicka, B. A.; Kumar, N.; Bellus, M. Z.; Chiu, H.-Y.; Zhao, H. Ultrafast and Spatially Resolved Studies of Charge Carriers in Atomically Thin Molybdenum Disulfide. *Phys. Rev. B* **2012**, *86*, 045406.

40. Schmitt-Rink, S.; Chemla, D. S.; Miller, D. A. B. Theory of Transient Excitonic Optical Nonlinearities in Semiconductor Quantum-Well Structures. *Phys. Rev. B* **1985**, *32*, 6601–6609.

41. Kleinman, D. A.; Miller, R. C. Band-Gap Renormalization in Semiconductor Quantum Wells Containing Carriers. *Phys. Rev. B* **1985**, *32*, 2266.

42. Park, S.; Mutz, N.; Schultz, T.; Blumstengel, S.; Han, A.; Aljarb, A.; Li, L. J.; List-Kratochvil, E. J. W.; Amsalem, P.; Koch, N. Direct Determination of Monolayer MoS_2 and WSe_2 Exciton Binding Energies on Insulating and Metallic Substrates. *2D Mater.* **2018**, *5*, 025003.

43. Liu, H.-L.; Shen, C.-C.; Su, S.-H.; Hsu, C.-L.; Li, M.-Y.; Li, L.-J. Optical Properties of Monolayer Transition Metal Dichalcogenides Probed by Spectroscopic Ellipsometry. *Appl. Phys. Lett.* **2014**, *105*, 201905.

44. Kumar, N.; Cui, Q.; Ceballos, F.; He, D.; Wang, Y.; Zhao, H. Exciton-Exciton Annihilation in $MoSe_2$ Monolayers. *Phys. Rev. B* **2014**, *89*, 125427.

45. Sun, D.; Rao, Y.; Reider, G. A.; Chen, G.; You, Y.; Brezin, L.; Harutyunyan, A. R.; Heinz, T. F. Observation of Rapid Exciton-Exciton Annihilation in Monolayer Molybdenum Disulfide. *Nano Lett.* **2014**, *14*, 5625–5629.

46. Poellmann, C.; Steinleitner, P.; Leierseder, U.; Nagler, P.; Plechinger, G.; Porer, M.; Bratschitsch, R.; Schuller, C.; Korn, T.; Huber, R. Resonant Internal Quantum Transitions and Femtosecond Radiative Decay of Excitons in Monolayer WSe_2. *Nat. Mater.* **2015**, *14*, 889–893.

47. Wen, X. W.; Chen, H. L.; Wu, T. M.; Yu, Z. H.; Yang, Q. R.; Deng, J. W.; Liu, Z. T.; Guo, X.; Guan, J. X.; Zhang, X.; Gong, Y. J.; Yuan, J. T.; Zhang, Z. H.; Yi, C. Y.; Guo, X. F.; Ajayan, P. M.; Zhuang, W.; Liu, Z. R.; Lou, J.; Zheng, J. R. Ultrafast Probes of Electron-Hole Transitions Between Two Atomic Layers. *Nat. Commun.* **2018**, *9*, 1859.

48. Ceballos, F.; Cui, Q.; Bellus, M. Z.; Zhao, H. Exciton Formation in Monolayer Transition Metal Dichalcogenides. *Nanoscale* **2016**, *8*, 11681–11688.

49. Steinleitner, P.; Merkl, P.; Nagler, P.; Mornhinweg, J.; Schuller, C.; Korn, T.; Chernikov, A.; Huber, R. Direct Observation of Ultrafast Exciton Formation in a Monolayer of WSe_2. *Nano Lett.* **2017**, *17*, 1455–1460.

50. Ceballos, F.; Zereshki, P.; Zhao, H. Separating Electrons and Holes by Monolayer Increments in van der Waals Heterostructures. *Phys. Rev. Mater.* **2017**, *1*, 044001.

51. Kumar, N.; Cui, Q.; Ceballos, F.; He, D.; Wang, Y.; Zhao, H. Exciton diffusion in monolayer and bulk $MoSe_2$. *Nanoscale* **2014**, *6*, 4915–4919.

52. Hoeben, F. J. M.; Jonkheijm, P.; Meijer, E. W.; Schenning, A. About Supramolecular Assemblies of Pi-Conjugated Systems. *Chem. Rev.* **2005**, *105*, 1491–1546.

53. Dexter, D. L. A Theory of Sensitized Luminescence in Solids. *J. Chem. Phys.* **1953**, *21*, 836–850.

54. Murphy, C. B.; Zhang, Y.; Troxler, T.; Ferry, V.; Martin, J. J.; Jones, W. E. Probing

Förster and Dexter Energy-Transfer Mechanisms in Fluorescent Conjugated Polymer Chemosensors. *J. Phys. Chem. B* **2004**, *108*, 1537–1543.

55. Kozawa, D.; Carvalho, A.; Verzhbitskiy, I.; Giustiniano, F.; Miyauchi, Y.; Mouri, S.; Neto, A. H. C.; Matsuda, K.; Eda, G. Evidence for Fast Interlayer Energy Transfer in $MoSe_2/WS_2$ Heterostructures. *Nano Lett.* **2016**, *16*, 4087–4093.

Graphical TOC Entry